REPORT DOCUMENTATION PAGE

Form Approved
OMB NO. 0704-0188

1. AGENCY USE ONLY (Leave Blank)	2. REPORT DATE	3. REPORT TYPE AND DATES COVERED
	03/31/04	Reprint (a) 07/22/02-03/31/04

4. TITLE AND SUBTITLE
Grain Size Hardening and Softening in Tungsten Carbide at Low Homologous Temperatures

5. FUNDING NUMBERS
DAAD19-02-1-0315

6. AUTHOR(S)
Hans Conrad and Jay Narayan

7. PERFORMING ORGANIZATION NAME(S) AND ADDRESS(ES)
North Carolina State University
Raleigh, NC 27695-7907

8. PERFORMING ORGANIZATION REPORT NUMBER
5-21616-2

9. SPONSORING / MONITORING AGENCY NAME(S) AND ADDRESS(ES)
U. S. Army Research Office
P.O. Box 12211
Research Triangle Park, NC 27709-2211

10. SPONSORING / MONITORING AGENCY REPORT NUMBER
41893.3-MS

11. SUPPLEMENTARY NOTES
The views, opinions and/or findings contained in this report are those of the author(s) and should not be construed as an official Department of the Army position, policy or decision, unless so designated by other documentation.

12 a. DISTRIBUTION / AVAILABILITY STATEMENT
Approved for public release; distribution unlimited.

12 b. DISTRIBUTION CODE

13. ABSTRACT (Maximum 200 words)

Data in the literature on the effect of grain size d in the range from cm to nm on the flow stress of WC are evaluated, including nanocrystalline materials prepared by a special pulsed laser ablation method. Three grain size regimes were identified: (a) Regime I, d=10^-2 to 0.5x10^-6, (b) Regime II, d=0.5x10^-6-10^-8 m and (c) Regime III, d<10^-8 m. Grain size hardening occurred in Regime I and II and softening in Regime III. Both straight and tangled dislocations were observed in Regime I. The major influence of grain size in Regime I could result from either its effect on the total dislocation density or the pile-up of dislocations. Insufficient data are available for Regime II to draw any positive conclusions regarding the governing mechanism. Analysis of the grain size softening in Regime III according to our grain boundary shear model yielded a reasonable activation volume but a lower-than-expected activation energy. The lower energy could be due to the presence of the amorphous NiAl film at the grain boundaries, employed to obtain the nanocrystalline grain size.

14. SUBJECT TERMS
tungsten carbide, grain size, nanocrystalline, flow stress, dislocations

15. NUMBER OF PAGES
8

16. PRICE CODE

17. SECURITY CLASSIFICATION OR REPORT	18. SECURITY CLASSIFICATION ON THIS PAGE	19. SECURITY CLASSIFICATION OF ABSTRACT	20. LIMITATION OF ABSTRACT
UNCLASSIFIED	UNCLASSIFIED	UNCLASSIFIED	UL

NSN 7540-01-280-5500

Standard Form 298 (Rev.2-89)
Prescribed by ANSI Std. 239-18
298-102

Enclosure 1

Electron Microscopy: Its Role in Materials Science (The Mike Meshii Symposium)
Edited by J.R. Weertman, M. Fine, K. Faber, W. King and P. Liaw TMS (The Minerals, Metals & Materials Society), 2003

GRAIN SIZE HARDENING AND SOFTENING IN TUNGSTEN CARBIDE AT LOW HOMOLOGOUS TEMPERATURES

Hans Conrad and Jay Narayan

Materials Science and Engineering Department
North Carolina State University
Raleigh, NC 27695-7907

Abstract

Data in the literature on the effect of grain size d in the range from cm to nm on the flow stress of WC are evaluated, including nanocrystalline materials prepared by a special pulsed laser ablation method. Three grain size regimes were identified: (a) Regime I, $d=10^{-2}$ to 0.5×10^{-6} m, (b) Regime II, $d=0.5\times10^{-6}$-10^{-8} m and (c) Regime III, $d<10^{-8}$ m. Grain size hardening occurred in Regimes I and II and softening in Regime III. Both straight and tangled dislocations were observed in Regime I. The major influence of grain size in Regime I could result from either its effect on the total dislocation density or the pile-up of dislocations. Insufficient data are available for Regime II to draw any positive conclusions regarding the governing mechanism. Analysis of the grain size softening in Regime III according to our grain boundary shear model yielded a reasonable activation volume, but a lower-than-expected activation energy. The lower energy could be due to the presence of the amorphous NiAl film at the grain boundaries, employed to obtain the nanocrystalline grain size.

Introduction

Reducing the grain size of crystalline solids provides the potential of increasing their strength and/or their ductility. This subject has become of special importance in recent years because of the development of methods for producing materials with grain sizes in the submicron and nanometer range. In prior work the present authors investigated the mechanisms responsible for the effect of grain size from millimeters down to nanometers on the flow stress of FCC Cu [1] and CPH Zn [2, 3]. Three grain size regimes were identified: (a) Regime I, $d\approx10^{-6}$-10^{-3} m, (b) Regime II, $d=10^{-3}$-10^{-6} m and (c) Regime III, $d<10^{-8}$ m. Grain size hardening occurred in Regimes I and II and grain size softening in Regime III. Intragranular dislocations were proposed to be active in both Regimes I and II, but only grain boundary shear in Regime III. Grain boundary shear had previously been proposed for the grain size softening reported for a number of metals and compounds [4]. The existence of grain size softening in materials with a nanometer grain size has however been questioned [5] in view of possible imperfections in such materials produced during processing including texture, a non-uniform grain size and porosity. However, the Zn films considered in Refs. 2 and 3, were produced by a special pulsed laser ablation-vapor deposition technique [6] which gave material free of such undesirable features ("artifacts") and confirmed grain size softening in nanocrystalline materials.

"Artifact-free" tungsten carbide (WC) films have recently been produced using a novel processing technique [6, 7], whereby pulsed laser deposition of WC in conjunction with a few monolayers of NiAl is used to control the grain size in the range of 6 to 35 nm. Microstructures of the WC films observed by HRTEM are shown in Figs. 1. To be noted is the uniform and texture-free (indicated by electron diffraction) nanometer grain size with no evidence of porosity, but with an amorphous layer of NiAl atoms at the grain boundaries. The hardness H of the films was measured employing a nanoindentation technique [8]. These hardness values

along with data in the literature provided the opportunity to evaluate the effect of grain size over a wide range on the flow stress of WC. This then was the objective of the present paper.

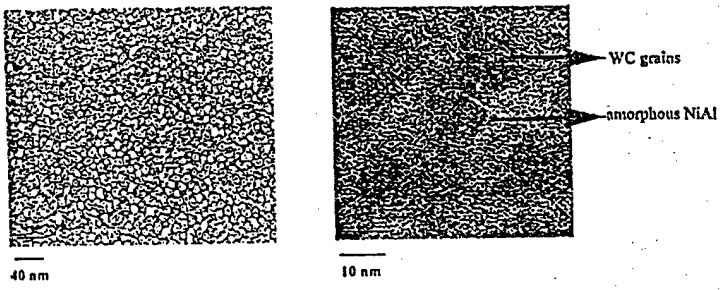

Fig. 1. HREM micrographs of a WC film fabricated by pulsed laser ablation. From Venkatesan et al. [7].

Data

The crystal structure of WC is simple hexagonal (Fig. 2) with lattice constants a=0.2906 nm and c=0.2837 nm giving c/a=0.976. The dominant slip system is $\{10\bar{1}0\}[11\bar{2}3]$, i.e. plastic deformation occurs by slip on the prism plane by the motion of dislocations with a Burgers vector $b=c+a=4.06\times10^{-10}$ m (i.e. $b=1/3\ [11\bar{2}3]$) [10-12]. The $1/3[11\bar{2}3]$ dislocations are dissociated into two partials, each with $b=1/6[11\bar{2}3]$ separated by a stacking fault. As pointed out by Hibbs and Sinclair [11], the $1/6\ [11\bar{2}3]$ partial Burgers vector could also give rise to b=[0001] and $b=1/3[11\bar{2}0]$, but these reactions would be energetically less favorable than for dislocations with $b=1/3\langle11\bar{2}3\rangle$ to dissociate into $b_1=b_2=1/6\langle11\bar{2}3\rangle$. Further, since the <0001> directions are the only vectors common to more than one prism plane, cross slip becomes a difficult process.

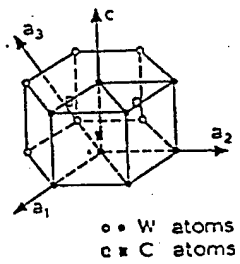

Fig. 2. Crystal structure of WC. The solid symbols define the unit cell. From Exner [9].

Fig. 3. TEM of the deformed region around an indentation in a WC-6 wt. % Co alloy showing the movement of the dislocations in the carbide grain. From Rowcliffe et al [16].

The slip lines in deformed WC single crystals are relatively straight and a high density of stacking faults exist [11]. The Knoop hardness (KNH) values measured by French and Thomas [12] on the basal plane varied only slightly with orientation, ranging from 22 GPa to 24.6 GPa at room temperature. In contrast, marked anisotropy occurred for measurements on the prism plane, the KHN values ranging from 9.8 GPa to 23.5 GPa. Lee [13] reported KHN values of 7.5 GPa to 17.5 GPa for measurements on the prism plane and 19 GPa on the basal plane. In comparison, he obtained a value of 23 GPa for polycrystalline WC prepared from $\sim 1\times10^{-6}$ m size powder by hot pressing. A value of 18 GPa was reported by Miyoshi and Hara [14] for polycrystalline WC with a grain size $d\approx10^{-2}$ m.

The deformation produced by indentation of the WC grains in cemented tungsten carbides (i.e., WC-Co alloys) is similar to that in polycrystalline WC prepared without a binder [15, 16]; an example of the dislocation structure in a WC-Co alloy is given in Fig. 3. In compression tests, the initial density of straight dislocation $\rho\approx10^{12}$ m^{-2} in the as-sintered WC grains multiplied and then took on a more complex arrangement, Fig. 4. Stacking faults were observed in both the as-sintered and deformed conditions.

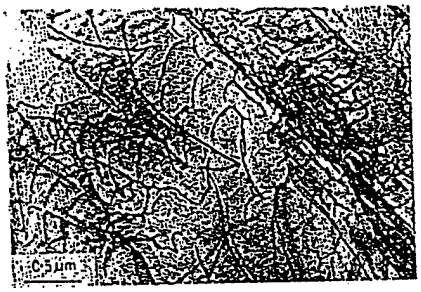

Fig. 4. Dislocation structure in a WC-Co alloy deformed ~1% in compression. From Sarin and Johanneson [17].

Lee and Gurland [18] established the following relationship for the hardness H_c of cemented carbides

$$H_c=H_{WC}V_{WC}C+H_m(1-V_{WC}C) \quad kg/mm^2 \qquad (1)$$

where $H_{WC}=1382+23.1d_{WC}^{-1/2}$ is the hardness of the carbide phase, d_{WC} is the carbide particle size, V_{WC} its volume fraction, C its contiguity and $H_m=304+12.7\lambda^{-1/2}$ is the hardness of the binder phase, λ is the binder mean free path. Hence, knowing H_c, d_{WC}, V_{WC}, C and λ for a given composite, one can calculate the value of H_{WC} as a function of d_{WC}. H_{WC} can also be obtained by extrapolating H_c vs Co content to zero Co.

A Hall-Petch plot of the effect of grain size d_{WC} on the hardness H of WC is presented in Fig. 5. The solid squares represent the laser ablated films corresponding to Fig. 1. For the compression tests, $H=3\sigma$, where σ is the yield stress.The plot reveals three regimes: (a) Regime I, $d^{-1/2}=(0\text{-}1.5)\times10^3$ m$^{-1/2}$, (b) Regime II, $d^{-1/2}=(1.5\text{-}9)\times10^3$ m$^{-1/2}$ and (c) Regime III, $d>9\times10^3$ m$^{-1/2}$. All of the data however lie within the range of the hardness of single crystals deformed by $\{10\bar{1}0\}\langle11\bar{2}3\rangle$ slip. Fig. 6 gives a log-log plot of the flow stress $\sigma=H/3$ vs. the carbide grain

size for the same data as in Fig. 5. Again, three regimes are indicated, all within the bounds of the stress for slip in single crystals.

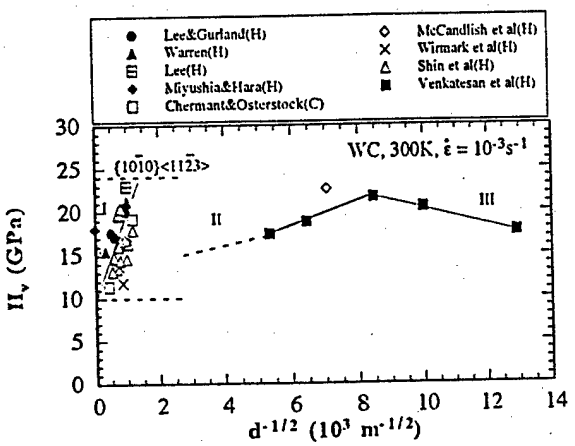

Fig. 5. Hall-Petch plot of the effect of grain size on the hardness of WC. Data from Refs. 13, 18-25. Filled symbols are from polycrystalline WC, open symbols from WC-Co alloys. Filled squares correspond to material with microstructure given in Fig. 1. (H) is hardness test, (C) is compression test.

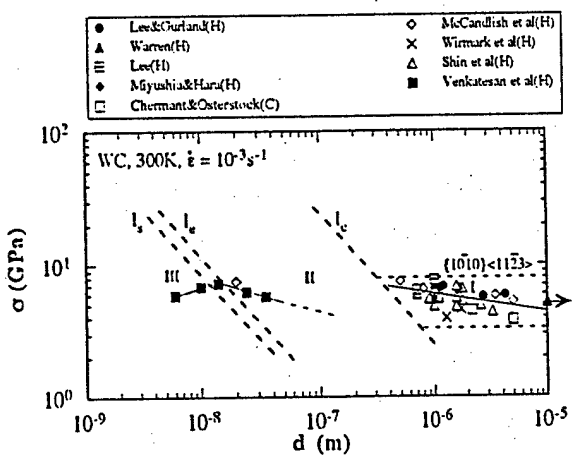

Fig. 6. Log flow stress σ vs. log grain size d of WC, same data as in Fig. 5.

Mechanisms

Regime I: The effect of grain size on the hardness of WC in this regime is in keeping with the Hall-Petch relation [26, 27] $\sigma=\sigma_i+k_{H\text{-}P}d^{-1/2}$, where σ_i is the lattice friction stress, or the flow stress of single crystals, and $k_{H\text{-}P}$ the Hall-Petch constant representing the additional effect of grain boundaries. Two dislocation models have been proposed for the Hall-Petch equation: (a) the pile-up of dislocations at grain boundaries [26-28] and (b) the excess of dislocations resulting from the reduction of the free slip distance by the grain size and the accomodation of slip in the vicinity of the boundaries, i.e. the work hardening model [29, 30]. The dislocation structure in Fig. 3 can be taken to support the pile-up model, while that in Fig. 4 the work hardening model.

Of further interest are the rate controlling mechanisms pertaining to σ_i and $k_{H\text{-}P}$, which correspond to the effects of temperature and strain rate on these parameters. The effects of temperature on the hardness of single crystals of WC, polycrystalline WC ($d_{WC}\approx 1$ μm) and cemented WC-6 wt.% Co ($d_{WC}\approx 1$ μm) are presented in Fig. 7. To be noted is that the hardness of the single crystals (which represents σ_i and $\{10\bar{1}0\}\langle 11\bar{2}3\rangle$ slip) has a strong temperature dependence beginning already at room temperature. In contrast, the hardness of the two polycrystalline materials exhibits a relatively weak temperature dependence up to about 600°C, following which a rapid decrease occurs. The strong temperature dependence is characteristic of a high Peierls-Nabarro stress, while the weak dependence is characteristic of an athermal process such as the long-range interaction between dislocations. The results in Fig. 7 along with the microscopy observations in Figs. 3 and 4 thus suggest that in the vicinity of room temperature σ_i is governed by the thermally-activated overcoming of a high Peierls-Nabarro stress and that $k_{H\text{-}P}$ reflects either relatively athermal activation of slip in the neighboring grain due to a pile-up of dislocations or an increase in total dislocation density due to the grain boundaries. Some support that thermally-activated overcoming of the Peierls-Nabarro stress is rate-controlling in polycrystalline WC-Co alloys below 1100°C is provided by the low value ($10\text{-}50b^3$) of the apparent activation volume $v=kT\partial\ln\dot{\varepsilon}/\partial\sigma$ obtained in stress relaxation tests [31].

Regime II: In metals the separation of Regimes I and II corresponded to the absence of a dislocation cell structure in Regime II compared to its existence in Regime I [1-3]. The limiting cell size λ_c in metals and ceramics is given by [32] $\lambda_c=\alpha_c\mu b/\sigma$ where $\alpha_c\approx 23$, σ the uniaxial flow stress, μ the shear modulus and b the Burgers vector. The line corresponding to this equation (taking $b=4.06\times10^{-10}$ m and $\mu=3/8E=265$ GPa [33]) is included in Fig. 6. To be noted is that all of the data points representing Regime I lie to the right of this line and those representing Regime II to the left. This suggests that the complex dislocation structure shown in Fig. 4 may not occur in Regime II. More data are however needed to confirm that the separation of the two regimes is indeed defined by the occurrence or absence of a dislocation cell-type structure.

The present authors are not aware of any data on the plastic deformation kinetics (i.e., the effects of temperature and strain on the flow stress) in Regime II in WC which could provide insight into the rate-controlling mechanism. Possibilities include: (a) overcoming the Peierls-Nabarro stress and (b) grain boundary shear produced by dislocation pile-ups, similar to what appeares to occur in Cu [1].

Regime III: The separation distance between dislocations due to their elastic interactions is given by [28] $\lambda_s=\frac{\mu b}{2\pi\tau}$(screw) and $\lambda_e=\frac{\mu b}{2\pi(1-\nu)\tau}$(edge) where τ is the resolved shear stress, μ the shear modulus and ν Poissons ratio. Hence, with decrease in grain size a limit will be

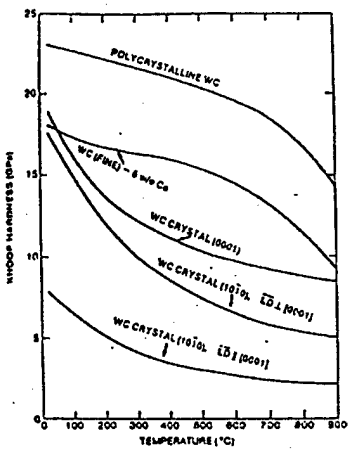

Fig. 7. Temperature dependence of the hardness of several tungsten carbide forms. WC crystal refers to single crystals; WC (fine)-6w/o Co to cemented carbide with ~1 μm grain size; Polycrystalline WC to sintered WC (d≈1 μm) without binder. LD indicates direction of the long axis of the Knoop indentor. From Lee [13].

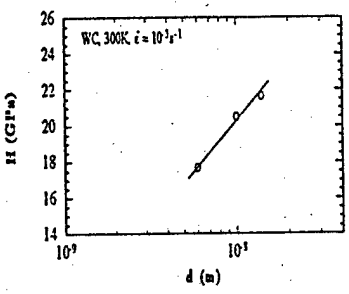

Fig. 8. Hardness vs. log WC grain size d for Regime III. Data from Venkatesan et al [7].

reached whereby the required separation of dislocations will be larger than the grain size. The limiting separations for WC are given by the lines labeled λ_s and λ_e in Fig. 6, taking b=4.06× 10^{-10} m, μ=265 GPa, ν=1/3 and τ=σ/5. They intersect the plot of log σ vs. log d_{WC} in the vicinity where grain size softening begins and thereby indicate that the deformation mode in Regime III is not by dislocations. The present authors propose that the plastic deformation mode responsible for the grain size softening in Regime III is grain boundary shear given by [4]

$$\dot{\gamma}=\frac{2\delta v_D}{d}\sinh\left(\frac{\tau_e v^*}{kT}\right)\exp-\left(\frac{\Delta F^*}{kT}\right) \tag{2}$$

where $\dot{\gamma}$ is the shear rate, δ is the grain boundary width, $v_D \approx 10^{13}$ s^{-1} the Debye frequency, d the mean linear intercept grain size, $\tau_e=\tau-\tau_c$ the effective shear stress, τ_c a critical or back stress, v^* the activation volume pertaining to the thermally-activated grain boundary shear event and ΔF^* the corresponding Helmholtz free energy. Normally, one expects that ΔF^* may be approximately equal to Q_b, the activation energy for grain boundary diffusion. Assuming that $\tau_e v^* >> kT$, taking the logarithm of Eqn. 4 and rearranging, we obtain

$$\tau_e=\frac{kT}{v^*}\left[\ln\left(\frac{\dot{\gamma}}{\delta v_D}\right)+\frac{\Delta F^*}{kT}\right]+\frac{kT}{v^*}\ln d_{WC} \tag{3}$$

Hence, providing $\tau_c \approx 0$ a plot of $H(=3\sqrt{3}\,\tau)$ vs. log d should be a straight line whose slope yields v^* and intercept ΔF^*. Such a plot is given in Fig. 8, from which one obtains $v^*=3.8\times10^{-30}$ m^3 and $\Delta F^*=101$ kJ/mole. The value of v^* is reasonable. However, the value of ΔF^* is much smaller than expected for grain boundary diffusion of either W or C in WC (~300 kJ/mole) [34, 35]. One possibility for the lower value of ΔF^* for the present material is the amorphous NiAl layer deposited at the grain boundaries during the fabrication of the nanocrystalline WC films.

Summary and Conclusions

Data in the literature on the effect of grain size d in the range of nm to cm on the flow stress and corresponding microstructure of WC is evaluated. Included is nanocrystalline WC prepared using a special pulsed laser ablation technique, which gave material free of "undesirable artifacts" and which exhibited grain size softening. The grain size data suggest three regimes: (a) Regime I, $d=10^{-2}$-0.5×10^{-6} m, (b) Regime II, $d=0.5\times10^{-6}$-10^{-5} m and (c) Regime III, $d<10^{-5}$ m. Grain size hardening occurred in Regime I and II and grain size softening in Regime III.

Both straight and tangled dislocations were observed in Regime I and therefore the grain size hardening could result from either an increase in the total dislocation density with decrease in grain size or from the pile-up of dislocations. The flow stress data for Regime I fell within the boundary for which a dislocation cell structure is predicted.

Only very limited data are available for Regime II so that no positive conclusion regarding the governing mode or mechanism could be made for this regime.

An analysis of grain size softening in Regime III according to our grain boundary shear model gave an activation volume in accord with predictions but a much smaller activation energy. The lower energy could be due to the amorphous NiAl layer at the WC grain boundaries, which was employed to establish the nanometer grain size.

Acknowledgements

This research was sponsored by the Army Research Office Award DAAD190210315 with Dr. William Mullins as technical monitor. The authors acknowledge the assistance of Ms. R. O'Connell and Dr. K. Jung in preparation of the manuscript.

References

1. H. Conrad, "Grain size dependence of the plastic deformation kinetics in Cu," *Mater. Sci. Eng.*, in print.
2. H. Conrad and J. Narayan, *Appl. Phys. Lett.* 81 (2002) 2241.
3. H. Conrad and J. Narayan, "Mechanisms for grain size hardening and softening in Zn," *Acta Mater.*, in print.
4. H. Conrad and J. Narayan, *Scripta Mater.* 42 (2000) 1025.
5. C. Koch and J. Narayan, in *Mater. Res. Soc. Symp. Proceed. vol. 634*, Materials Research Society, Warrendale, PA (2001) p. B5.1.
6. J. Narayan, J. *Nanoparticle Res.* 2 (2000) 91.
7. R. K. Venkatesan, A. Kvit, Q. Wei and J. Narayan, in *Mater. Res. Soc. Symp. Proceed. vol. 634*, Materials Research Society, Warrendale, PA (2001) p. B6.1.1.
8. W. C. Oliver and G. M. Pharr, *J. Mater. Res.* 7 (1992) 1564.

9. H. E. Exner, Review 243, *Int. Metals Reviews* No. 4 (1979) 149.
10. S. B. Luyckx, *Acta Metall.* 18 (1970) 233.
11. M. K. Hibbs and R. Sinclair, *Acta Metall.* 29 (1981) 1645.
12. D. N. French and D. A. Thomas, *TMS-AIME* 233 (1965) 950.
13. Minyoung Lee, *Metall. Trans. A* 14A (1983) 1625.
14. Miyushi and A. Hara, *Funtai Oyobi Fummatsuyakin* 12 (1964) 24.
15. V. Jayaram, R. Sinclair and D. J. Rowcliffe, *Acta Metall.* 31 (1983) 373.
16. D. J. Rowcliffe, V. Jayaram, M. Hibbs and R. Sinclair, in *Science of Hard Materials 3*, V. K. Sarin, ed. Elsevier, New York (1988) p.299.
17. V. K. Sarin and T. Johanneson, *Met. Sci.* 9 (1975) 472.
18. H. C. Lee and J. Gurland, *Mater. Sci. Eng.* 33 (1978) 125.
19. L. E. McCandlish, V. Kororkian, K. Jia and T. E. Fisher, *Adv. Powder Met. and Particulates-1994*, Vol. 5, Metal Industries Federation, Princeton, NJ (1994) p. 329.
20. P. Seegopaul, L. E. McCandlish and F. M. Shinneman, *Int. J. Refractory Metals and Hard Materials* 15 (1997) 133.
21. Y. Shin, W. Cao, G. Sargent and H. Conrad, *Mater. Sci. Eng. A*105/106 (1988) 377; Science of Hard Materials 3, V. K. Sarin, ed., Elsevier, New York (1988) p. 377.
22. G. Wirmark, C. Chatfield and G. L. Dunlop, in *Science of Hard Materials 2*, Inst. Physics Conf. Series No. 75, Adam Hilger Ltd., Boston (1986) p. 669.
23. J. L. Chermont and F. Osterstock, *Powder Met. Ind.* 11 (1979) 106.
24. L. E. McCandlish, Kang-Jia and T. E. Fisher, in *Nanophase and Nanocomposite Materials*, Mater. Res. Soc., Pittsburgh, PA (1997) 303.
25. R. Warren in Proc. 4th Risø Int. Symp. Metall. Mater. Sci., Deformation of Multi-phase and Particle Containing Materials, Risø National Lab. (Sept. 1983) p.1.
26. E. O. Hall, *Proc. Phys. Soc.* London 64B (1951) 747.
27. N. Petch, *J. Inst. Met.* 174 (1955) 25.
28. H. Cottrell, *Dislocations and Plastic Flow in Crystals*, Oxford Univ. Press, London (1953).
29. H. Conrad, in *Electron Microscopy and Strength of Crystals*, G. Thomas and J. Washburn, eds., Interscience, New York (1961) p. 289; in Ultrafine-grain Metals, J. Burke and N. Reed, eds. Syracuse Univ. Press, Syracuse (1970) p. 213; Mater. Sci. Eng. 2 (1967) 157.
30. M. F. Ashby, *Phil. Mag.* 21 (1970) 399.
31. S. R. Schenck, R. J. Gottschall and W. S. Williams, *Mater. Sci. Eng.* 32 (1978) 229.
32. S. V. Raj and G. M. Pharr, *Mater. Sci. Eng.* 81 (1986) 217.
33. R. Reeber and K. Wang, *J. Am. Ceram. Soc.* 82 (1999) 129.
34. C.P. Bushmer and P. H. Crayton, *J. Mater. Sci.* 6 (1971) 981.
35. D. Treheux, J. Dubois and G. Fantuzzi, *Ceram. Int.* 7 (1981) 142.